Biochemistry and Biophysics Reports 40 (2024) 101877

Contents lists available at ScienceDirect

Biochemistry and Biophysics Reports

journal homepage: www.elsevier.com/locate/bbrep

Application of liposomal nanoparticles of berberine in photodynamic therapy of A549 lung cancer spheroids

Kave Moloudi, Heidi Abrahamse, Blassan P. George *

Laser Research Centre (LRC), Faculty of Health Sciences, Doornfontein Campus, 2028, University of Johannesburg, Johannesburg, South Africa

ARTICLE INFO

Keywords:
Liposomal nanoparticles
Berberine
Photodynamic therapy
Photosensitizer
Laser
Lung cancer
Spheroid cell culture

ABSTRACT

Application of liposomes is a critical strategy in drug delivery and increase cellular uptake of drugs having low water solubility. Berberine (BBR) is a bioactive compound found in several plants, including Goldenseal, Barberry, and Oregon grape. It has garnered attention for its various health benefits, particularly in metabolic health and antimicrobial activity. However, one of the challenges associated with BBR is its water solubility. Moreover, BBR has photosensitizing potential via absorbance of light and generation of free radicals. Hence, to improve water solubility and bioavailability, one of the important strategies employed is using lipid-based carriers to enhance solubility. In this study we employed liposomes to deliver BBR in A549 lung cancer spheroid cells to enhance photodynamic therapy efficacies. Results from the EDS and UV–Vis spectroscopy revealed that the BBR had been loaded onto liposomes, with three peaks appearing between 250 and 450 nm. Morphology of Lipo@BBR nanocomplex was in wavy crest shape and the size was 56.99 ± 3.74 nm in SEM and TEM analysis, respectively. FTIR data illustrated that Lipo@BBR has four significant peaks at 1250, 1459, 1736, and 2907 cm^{-1}. DLS data showed that Lipo@BBR has a negative surface charge with a −10.7 Zeta Potential (mV). Additionally, based on Zetasizer measurements, the size of Lipo@BBR complex was 82.7 ± 6.5. Cytotoxicity assay investigation with MTT assay presented that IC_{50} of Lipo@BBR in PDT was 10 ± 0.5 μg/mL that led to a volume reduction of the A549 spheroids after five sessions of PDT fractionation (total light dose was set at 25 J/cm^2). qPCR and immunofluorescence results demonstrated that Lipo@BBR increases the BAX/BCL2 ratio in A549 spheroid cells, hence improving PDT efficiency. In conclusion, our results illustrated that safe dose of Lipo@BBR (10 ± 0.5 μg/mL) in PDT fractionation protocol can be one of the strategies to suppress the tumor volume and cell death proliferation. Authors recommend using Lipo@BBR nanocomplex in PDT fractionation as well as more *in vivo* investigation is warranted.

1. Introduction

Photodynamic therapy (PDT) is a type of cancer treatment that uses a combination of a photosensitizing drug and a specific type of light to kill cancer cells. The process involves administering a photosensitizing agent, which is absorbed by the cancer cells, followed by exposure to a specific wavelength of light. This interaction between the drug and the light produces reactive oxygen species (ROS) such as singlet oxygen and other free radicals that kills nearby cells. PDT can be used to treat early-stage tumors that are localized within the lungs or the lining of the chest cavity, PDT [1-3].

Oxygen level of tumor plays a crucial role in PDT which the interaction between the photosensitizer, light, and oxygen generates ROS, which are toxic to cancer cells. Therefore, ensuring adequate oxygen supply to the treatment area is essential for the effectiveness of PDT [4]. One of the challenges in PDT is oxygen depletion of tumor after each irradiation which leading to reduction of treatment efficiency. In some cases, supplemental oxygen may be provided to optimize the therapy's outcomes [5,6]. However, as a strategy to overcome this challenge, fractionation PDT can be used, which also minimizes the side effects of normal tissue [7,8]. Fractionation treatment refers to the practice of dividing a treatment into smaller and more manageable doses, resulting to reduce the risk of side effects and allow healthy tissues to recover between treatments. Fractionated PDT involves delivering the photosensitizing drug and light treatment in multiple sessions, spaced out over a period of time. This approach allows for a more controlled and targeted delivery of the photosensitizer, as well as enhanced tissue oxygenation and recovery between treatment sessions. Therefore,

* Corresponding author.
E-mail address: blassang@uj.ac.za (B.P. George).

https://doi.org/10.1016/j.bbrep.2024.101877
Received 16 October 2024; Received in revised form 8 November 2024; Accepted 14 November 2024

fractionation in PDT can offer several benefits, including, reduced side effects, enhanced efficacy, improved tissue oxygenation [9-11].

Berberine (BBR) is a natural and anticancer compound found in several plants, including the barberry, goldenseal, and Chinese goldthread [12,13]. Moreover, BBR is a potent photosensitizer for PDT purpose that it can absorbs light at 344–422 nm wavelength (a maximum absorption is 418 nm) and produce ROS such as singlet oxygen ($^1O_2$), superoxide Anion ($O_2^{\bullet-}$), hydrogen peroxide (H_2O_2), hydroxyl radical ($^{\bullet}OH$) and peroxyl radicals ($ROO^{\bullet}$), leading oxidative damage, DNA damage, G2/M cell cycle arrest and apoptosis [14-16]. Consequently, ROS can lead to intrinsic apoptotic pathway via mitochondrial dysfunction, causing the release of cytochrome *c* from the mitochondria into the cytosol and activating caspases (caspase-9 and caspase-3). Further, some studies suggested that ROS can also activate death receptors on the cell surface, leading to the extrinsic apoptotic pathway [17,18]. Several studies reported that the nanoformulations of BBR can improve cellular uptake and treatment outcomes more than its free form (powder) [19,20]. In addition, the nanoformulation of BBR presents a promising approach in cancer therapy by enhancing its bioavailability, targeting capabilities, and overall therapeutic efficacy while potentially reducing side effects [21,22]. Nanoliposomes offer several unique advantages in comparison other nanoparticle systems (polymeric nanoparticles, and metal nanoparticles) such as biocompatibility and biodegradability, encapsulation both hydrophilic (water-soluble) and hydrophobic (lipid-soluble) drugs, controlled release and targeted delivery. Liposomes as lipid-based nanoparticles can provide a cutting-edge method to transport active molecules and new drug delivery into cancer cells, and several formulations of them such as Doxil, Visudyne and Myocet as photosensitizer and chemotherapeutic drugs are approved by Food and Drug Administration (FDA) and now being used in clinical practice [23-25].

Hence, in this study, we used liposomal berberine nanocomplex (Lipo@BBR) in combination with 405 nm laser on A549 lung cancer spheroid cells.

2. Method and materials

2.1. Materials

BBR chloride (10006427, powder , Purity >95 %), dimethyl sulfoxide (DMSO), 3-(4,5-dimethylthiazol-2-yl)-2,5-diphenyltetrazolium bromide (MTT) (11465007001), cholesterol (Chol) (C8667), 1,2-Distearoyl-sn-glycero-3-phosphocholine (DSPC) (P1138-1G), citrate gold nanoparticles (AuNPs) (741957), Gibco Dulbecco's Modified Eagle Medium (DMEM) (D5796), Chloroform (C2432), methanol (439193), fetal bovine serum (FBS), phosphate buffered saline (PBS), 96-well ultra-low attachment plates (174929), 4 % paraformaldehyde and crystal violet (C6158-50G, Purity >90 %) were purchased from Sigma (USA) and ThermoFisher in Johannesburg, South Africa.

2.2. Synthesis and characterization of Lipo@BBR nanocomplex

Loading BBR into liposomes using the thin-film method is a popular approach for enhancing its solubility and bioavailability. Lipo@BBR were synthesized by the thin-film hydration method [26,27]. Briefly, mixture of DSPC (90 mg/mL), Chol (30 mg/mL) at 3:1 ratio, BBR (20 μM or 0.20 mg) were dissolved in chloroform and methanol (4:1, v/v), then rotary evaporator (75 rpm at temperature 75 °C for 1 h) used to evaporate the extra solvent and form a thin lipid layer. After hydration medium with phosphate-buffered saline and gentle shake to facilitate the hydration of the lipid film and formation of liposomes, sonication (30 min) to achieve uniform liposome size was performed. Finally, samples were centrifuged (18000 for 10 min) to remove unencapsulated BBR and free lipids. Afterward, obtained nanoparticles stored at 8 °C for characterization. Transmission electron microscopy (TEM), scanning electron microscopy (SEM), energy-dispersive spectroscopy (EDS) using SEM (VEGA3 TESCAN), dynamic light scattering (DLS) using Malvern Instrument (Zetasizer software 7.03, Malvern, UK), FTIR (PerkinElmer Spectrum Version 10.03.02) and UV–Vis spectroscopy (Jenway, 7315 spectrophotometer) analyses for measuring size, morphology, stability and distribution (pH = 6.8), surface charge, absorption peak and encapsulation efficiency (EE%) of BBR were performed. EE of BBR on liposomes was quantified using the equation:

$$\%\ EE = \text{Amount of drug loaded} / \text{Initial amount of drug X } 100 \quad (1)$$

2.3. Cytotoxicity of Lipo@BBR nanocomplex before and after PDT

DMEM media containing 10 % FBS and 1 % Penicillin-Streptomycin (P4458) was used to seed A549 human lung cancer cells in 25-flask plates. After 80–90 % confluency was achieved, the cells were harvested and counted. To spheroid formation, cells were plated at density of 3×10^3 cells in 200 μL of growth media per well using 96-well spheroid microplates (4520). Spheroids growth and shapes were analyzed using inverted Olympus microscope (USA). MTT assay was used to evaluate Lipo@BBR toxicity at concentrations of 0–20 μg/mL on the A549 spheroid cells with and without laser at 5 J/cm^2 energy for 24 h. The groups included control (cells alone for dark toxicity), laser (cells alone), 2, 4, 6, 8, 10, 12, 14, 16 and 20 μg/mL with and without laser. In order to prepare single cells, A549 spheroid cells were disassociated with 200 μL TrypLE for 5 min, then the medium was discarded, and the cells were washed with PBS and 2×10^4 cells/mL seeded in 96-well polystyrene tissue culture plates. The cells were then placed in a humidified 5 % CO_2 incubator at 37 °C for overnight to attach. Following the incubation period, the medium was extracted, and each well was filled with 20 μL aliquots of MTT solution (5 mg/mL in PBS, Sigma, USA and plate re-incubated for 4 h at 37 °C. After carefully aspirating 100 μL of the supernatant culture media, 100 μL aliquots of DMSO were added to each well to dissolve the formazan crystals and incubated for 30 min. The culture plate was placed on a microplate reader (PerkinElmer, HH35940080 EN, Midrand, South Africa) and shook for 15 min, and absorbance was then measured at 540 nm. The cell viability rate was calculated as the percentage of MTT absorption as per the equation:

$$\%\ \text{Survival} = \text{Mean OD of sample} / \text{Mean OD of control} \times 100 \quad (2)$$

2.4. Photodynamic therapy (PDT)

A 405 nm diode laser was used for PDT and the laser parameters are summarized in Table 1. However, to determine the therapeutic efficiency of the Lipo@BBR in PDT, we used the maximum safe dose of Lipo@BBR (10 μg/mL) with various fractionations including compared with control (A549 spheroid cells alone), laser (A549 spheroid cells alone) at wavelength of 405 nm laser (5 J/cm^2 energy per session and total light dose was set at 25 J/cm^2). The A549 spheroid cells were exposed using a 1000 mA laser source (4210 Laser Source, Arroyo Instruments, LLC, CA, United States) and a 405 nm diode laser (National Laser Centre, South Africa, SN 070900108). The laser output power (mW) was measured by using a Power Meter (Coherent®, FieldMate, 1098297, Alp Applied Laser Power, South Africa) and a High-Sensitivity Thermopile Sensor PM3 (Coherent®, PM3, 1098336, ALP- Applied Laser Power, South Africa) used to calculate the laser exposure time based on

Table 1
The laser parameters are summarized.

Laser parameters	
Photosensitizer (PS)	Lipo@BBR
PS concentration (μM)	10 μg/mL
Laser type	semiconductor (diode)
Wavelength (nm)	405 nm
Wave emission	Continues
Fluence (J cm−2)	5

the fluence via equations of (3), (4) and (5). Afterward, the cells were seeded in a 96-multiwell non-adherent plate, at a concentration of 3×10^3 cells per well, and allowed to grow for 3 days; then the A549 spheroids were treated with IC_{50} of Lipo@BBR (10 μg/mL) in five PDT sessions (5 J/cm^2 in each session) for 24 h. The magnitude of the laser spot covered the entire 4 wells during exposure (diameter area was 3.4 cm or radius was 1.7 cm). The irradiation time (min) was calculated as follows:

$$\text{Intensity (W/cm}^2\text{)} = \text{Energy/Area} = 70 \times 10^{-3}\ \text{W} / 3.14 \times 1.7^2\ \text{cm} = 0.0077\ \text{W/cm}^2 \quad (3)$$

$$\text{Area} = \pi r^2 = 3.14\text{x}1.7^2 = 9.074\ \text{cm}^2 \quad (4)$$

$$\text{Exposure time (min)} = \text{Dose(J/cm}^2\text{)/Intensity (W/cm}^2\text{)} = 5\ /0.0077 = 10.82 \simeq 11\ \text{min} \quad (5)$$

2.5. Tumor volume and colony formation assay post-PDT

Diameter of A549 spheroids were measured before and after PDT. Then the volume curve of spheroid was drawn. Volume cells spheroids were measured by following equation:

$$V = 4/3\pi r^3, \text{ which } \pi = 3.14 \text{ and r is radius.} \quad (6)$$

Colony formation assay used to assess the ability of individual cells to proliferate and form colonies. The assay provides valuable information about the clonogenic potential of cells, which refers to their ability to grow and divide to form a visible colony. Hence, A549 spheroid cells were treated with IC_{50} (10 μg/mL) of Lipo@BBR in PDT (405 nm laser at energy of 5 J/cm^2 for five sessions). Then spheroids disassociated with 200 μL of TrypLE and number of 1000 cells were seeded in 6-multiwell (M8562) plate in DMEM and incubated for 12 days to proliferate and form colonies. After the incubation period, the cells are fixed with 5 % formaldehyde and stained with 0.5 % crystal violet dye that allows for the visualization of cell colonies. The resulting colonies are then counted by fluorescence microscope and ImageJ software (version1.48v). The colony formation was defined by a cell population of at least 50 cells.

2.6. Quantitative Polymerase Chain Reaction (qPCR) for apoptotic gene expression

Real-time Quantitative Polymerase Chain Reaction (RT-qPCR) was performed to compare the expression of apoptosis-related genes including Bax, Bcl-2 (as anti-apoptotic factor) and P53 for all groups including control (cells alone), laser (5 J/m^2) and, Lipo@BBR + laser. The isolation of the RNA samples were carried out using RNeasy kit (Whitehead Scientific, RSA, Qiagen, 74104) with QIA shredder homogenizers (Whitehead Scientific, RSA, Qiagen, 79654) from 1×10^6 cells of all groups according to the manufacturer's instructions. Then, quality and quantity of extracted RNA samples were assessed using the Qubit 3.0 Fluorometer (Invitrogen, USA). Based on the quality and quantity of extracted RNA, 200 ng/mL RNA was converted into cDNA using QuantiTect Reverse Transcription Kit (205311, QIAGEN, USA) according to the manufacturer's instructions. Primer3 software (version 0.4.0) was used to build the primer sequences for GAPDH, Bax, Bcl-2, and P53. To normalize the expression of target genes, GAPDH was employed as an internal control. The forward and reverse primer sequences for target amplification is given in Table 2. Finally, relative fold expression was determined using the $2^{-\Delta\Delta CT}$ ($\Delta\Delta CT$ = ΔCT treated - ΔCT untreated) method [28] and the cycle threshold (CT) values obtained from RT-qPCR.

2.7. Immunofluorescence (IF) assay

To determine apoptotic cell death mechanism of Lipo@BBR in PDT qualitative assessment of apoptotic proteins such as BAX, caspase-3 (CASP-3) and P53 was carried out with IF imaging. Briefly, after A549 spheroid cells treatment with IC_{50} of Lipo@BBR-mediated PDT for 24 h, spheroids disassociated with 200 μL of TrypLE and number of 10^5 cells were seeded in 6-MW plate with sterile glass coverslips containing 2 mL of complete DMEM medium. After 24 h, A549 cells were washed three times using PBS (1x), and fixed for 15 min using 1 mL of 5 % paraformaldehyde. Thereafter, cells were washed three times with ice-cold PBS (1x) to remove excess paraformaldehyde and permeabilized using 0.5 % Triton X100 (1 mL) at room temperature for 15 min and washed three times with PBS. Then to avoid non-specific binding and interactions of antibodies (Abs) cells incubated for 1 h with 1 mL of 1 % Bovine Serum Albumin (BSA) and washed twice using ice-cold PBS (1x). The anti-BAX (41162), anti-CASP-3 (C8487) and aniti-P53 (2527) antibodies were provided by Cell Signaling Technology (Johannesburg, South Africa). After the preparation of antibodies and disassociation of A549 spheroids, cells were seeded on coverslips and incubated for 24 h. Afterward cells washed three using PBS, ~200 μL of primary Abs was added onto the surface of the coverslips and incubated for 2 h at room temperature in the dark. Post-incubation, cells were washed three times to remove unbound primary Abs, then treated with 200 μL of reconstituted FITC-labeled secondary Abs (goat anti-mouse IgG-FITC conjugated (sc-2010) (Santa Cruz® Biotechnology) and incubated for 1 h at room temperature in the dark, After removing unbound secondary Abs from the cells with three ice-cold PBS (1x) washes, coverslips were stained for 5 min with 200 μL of 4′,6-diamidino-2-phenylindole (DAPI), and excess DAPI was removed with three PBS (1x) washes. Lastly, sterile microscopic glass slides with coverslips containing labeled cells were mounted and using an Olympus BX41 microscope, observed for the qualitative expression (fluorescent signals) of pro-apoptotic proteins such as BAX, CASP-3, and P53.

2.8. Data analysis

All experiments were performed three times ($n = 3$) and data average was calculated after each tests. The control groups and all treated groups were compared for the purpose of determining statistical significance using a one-way analysis of variance (ANOVA) (Tukey test). The statistical significances between the groups were analyzed using SPSS (Version 22). A p-value below 0.05 (***$p < 0.001$; **$p < 0.01$; *$p < 0.05$) considered as statistically significant. Results are represented as Mean ± Standard deviation (SD). Shortly, the basic concept behind ANOVA is to compare the variance (variability) within each group to the variance between the groups and SD helps to understanding the variability of the data within and between groups [29,30].

Table 2
The primer nucleotide sequences used for RT-qPCR.

Genes	Code number	Forward primer (5′-3′)	Reverse primer (5′-3′)	Product size (bp)
BAX	S212D, S212E	GGACGAACTGGACAGTAACATGG	GCAAAGTAGAAAAGGGCGACAAC	150
BCL2	S212F, S2130	ATCGCCCTGTGGATGACTGAG	CAGCCAGGAGAAATCAAACAGAGG	129
P53	S213G, S213H	CCTCAGCATCTTATCCGAGTGG	TGGATGGTGGTACAGTCAGAGC	153
GAPDH	S213B, S213C	GAGTCAACGGATTTGGTCGT	GACAAGCTTCCCGTTCTCAG	185

3. Results

3.1. Characterizations of Lipo@BBR

BBR was detected in the Lipo@BBR complex by Energy Dispersive Spectroscopy (EDS) analysis and SEM imaging (built-in software used) [31]. The morphological SEM image showed that the BBR drug is wavy crest shaped in the Lipo@BBR complex, (Fig. 1(A&B)). In addition, The TEM data showed that the loading of BBR on liposomes and the size of Lipo@BBR complex was 56.99 ± 3.74 nm, Fig. 1(C). According to the UV–Vis spectra Fig. 1(D), liposomes have a peak close to 210 nm wavelength while BBR has three peaks between 250 and 450 nm. The highest concentration of BBR co-loaded in the Lipo@BBR complex is 15 μM (89 ± 2 %). Additionally, FTIR data showed four absorbance peaks were visible in BBR around 1035, 1105, 1505, and 2850 cm^{-1}, respectively. Liposome and Lipo@BBR had four of the same significant peaks at 1250, 1459, 1736, and 2907 cm^{-1}, Fig. 1(E). Dynamic light scattering (DLS) data are shown in Fig. 1(F), showing that Lipo@BBR has a negative surface charge with a −10.7 Zeta Potential (mV). Based on Zetasizer measurements, the size of Lipo@BBR complex was 82.7 ± 6.5, as illustrated in Fig. 1(G).

3.2. Cytotoxicity of Lipo@BBR nanocomplex

Cytotoxicity of various concentrations of Lipo@BBR nanocomplex (contain 15 μM) before and post PDT evaluated with MTT assay (Fig. 2). Cell viability (%) pre-PDT for various groups including control (cells alone), 2 μg/mL, 4 μg/mL, 6 μg/mL, 8 μg/mL, 10 μg/mL, 12 μg/mL, 14 μg/mL, 16 μg/mL and 20 μg/mL was 100, 98.5, 98, 97.5, 97.01, 95.2, 91, 90.08, 88.60 and 82.25 %, respectively. However, Lipo@BBR in comparison with control group, did not show significant cytotoxicity in concentrations less than 10 μg/mL (concentrations<10 μg/mL) (*$p > 0.05$). Additionally, various concentrations of Lipo@BBR post-PDT (5 J/cm^2) reduced cell viability to 100, 98.5, 90, 87.5, 77.01, 48.2, 41, 36.08, 22.60 and 11.25 %, respectively. Hence, IC_{50} of Lipo@BBR post-PDT was 10 μg/mL (***$p < 0.001$). This concentration was used for further experiments in PDT.

3.3. Tumor volume and colony formation of A549 spheroids post-PDT

The tumor volume and colony formation of A549 spheroids post-PDT was observed using Olympus microscope. The volume of A549 spheroids at various fractionation doses (5 J/cm^2) was measured every session following PDT (24 h post-PDT). As can be seen from Fig. 3 (A and C), diameter of A549 spheroid from 825.23 μm (before treatment) reduced to 413.53 μm, using Lipo@BBR (10 μg/mL) in PDT at 25 J/cm^2. Thereafter, each session post-PDT, cell survival rates were observed using colony formation assay. However, the cell survival (%) for various groups including control (before treatment), laser alone (5 J/cm^2), 10 μg/mL + 5 J/cm^2, 10 μg/mL + 10 J/cm^2, 10 μg/mL + 15 J/cm^2, 10 μg/mL + 20 J/cm^2 and 10 μg/mL + 25 J/cm^2 was 100 ± 2, 91 ± 3, 52 ± 3, 44 ± 6, 35 ± 2, 28 ± 3 ad 23 ± 2 %, respectively, Fig. 3 (B and D).

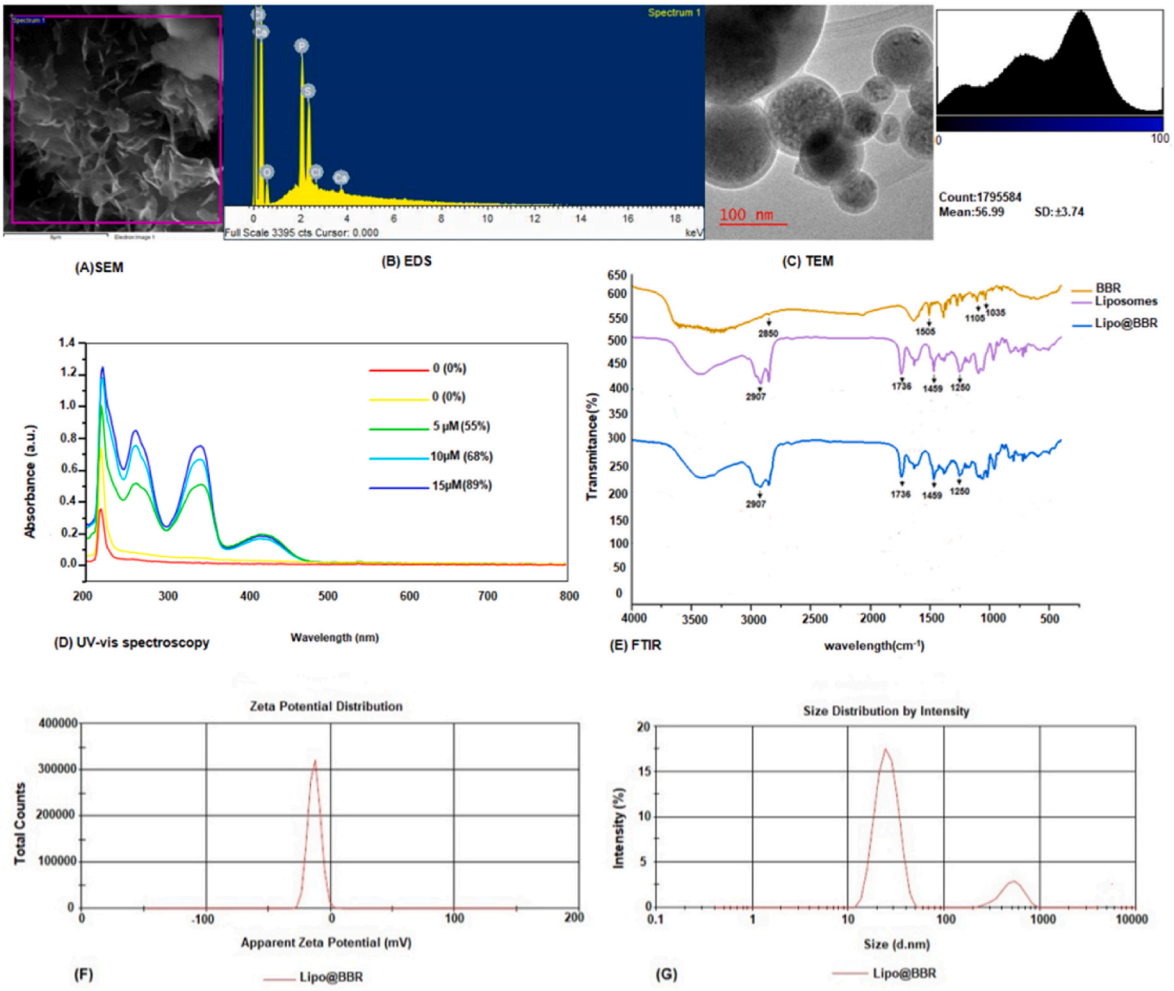

Fig. 1. Spectral characterization of Lipo@BBR. (A), (B) and (C) SEM image, EDS and TEM image. (D), UV–Vis spectroscopy and maximum BBR loading. (E), FTIR, (F), Zeta potential and (G), Zeta sizer analysis.

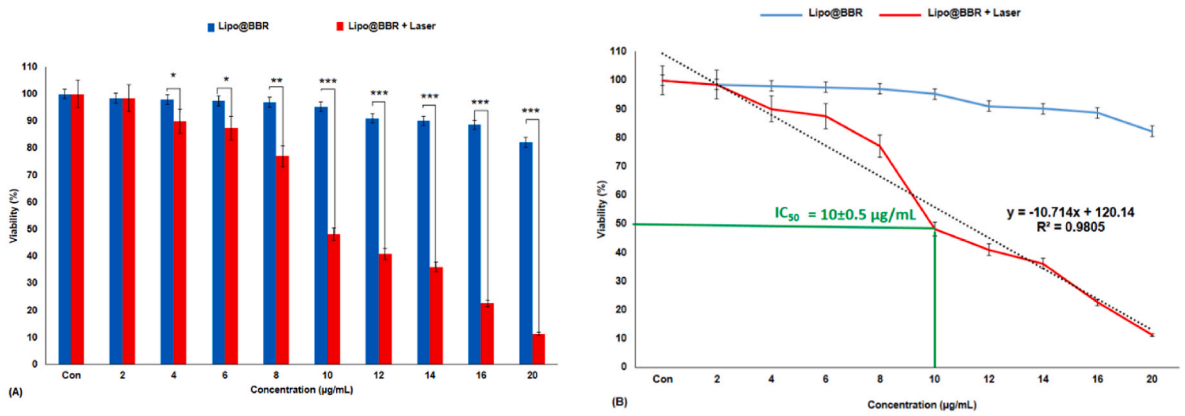

Fig. 2. (A), Cytotoxicity of Lipo@BBR (0–20 μg/mL) alone and post-PDT (5 J/cm^2). IC_{50} of Lipo@BBR in PDT was 10 μg/mL (*p < 0.05, **p < 0.01, ***p < 0.001). (B), regression plot ($R^2 = 0.9805$) and IC_{50} of Lipo@BBR post-PDT (10 ± 0.5 μg/mL).

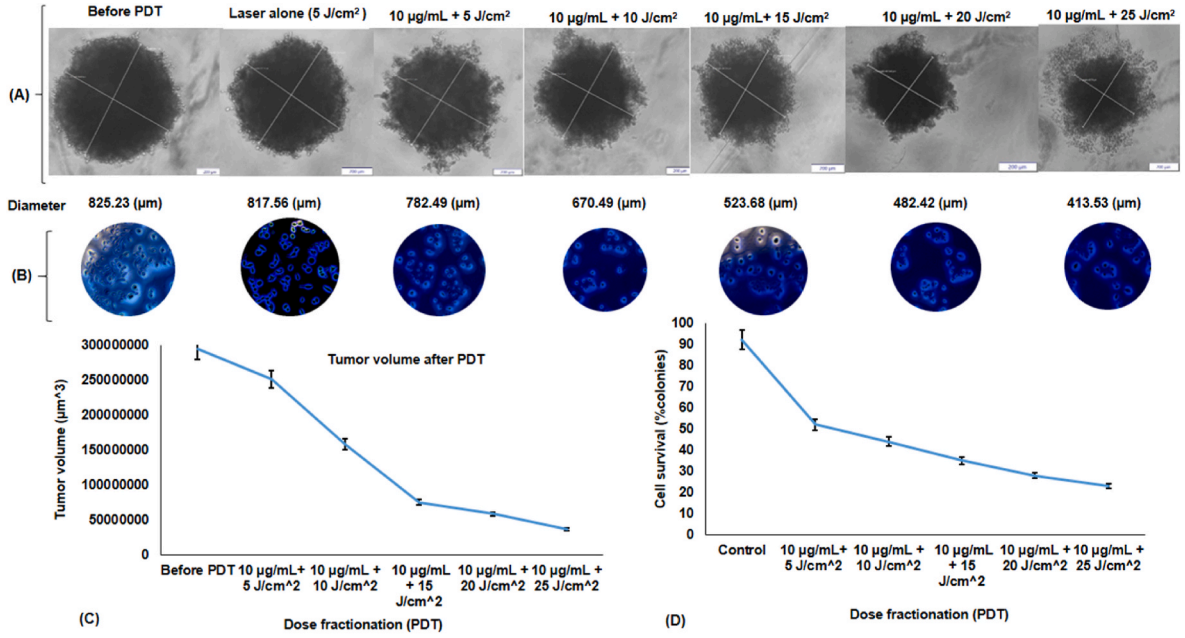

Fig. 3. (A), images and the size (μm) of A549 spheroid before and post-PDT in various sessions, (scale bars: 200 μm). (B), colonies before and post-PDT in various sessions (the cell population of 50 or more cells was used to define the colony). (C), Tumor volume curve post-PDT. (D), cell survival curve in various sessions of post-PDT.

3.4. Apoptotic genes expression in qPCR

To determine the apoptosis inducing effect of Lipo@BBR in PDT, the mRNA expression level of three apoptosis-related genes, BAX (as a pro-apoptotic gene), BCL2 (as an anti-apoptotic factor) and P53 (as a pro-apoptotic factor) were examined using the RT-qPCR. As shown in Fig. 4, Lipo@BBR in PDT significantly increased the expression of BAX and P53 and level of BCL2 decreased (*p < 0.05, **p < 0.01). However, the A549 spheroid cells treated with Lipo@BBR + laser illustrated 4.31 and 4.25 -fold increase in Bax and P53, respectively (for groups ***p < 0.01). While BCL2 expression decreased to 0.63-fold, compared to control group, respectively (*p < 0.05). Hence, the expression of BAX and P53 in PDT groups was significantly upregulated while, BCL2 anti-apoptotic factor was significantly downregulated in comparison with control and laser alone treated groups. Additionally, BAX/BCL2 ratio for Lipo@BBR + laser treated group reached 6.8 while for control and laser control groups observed at 1 and 1.19, respectively.

3.5. Immunofluorescence assay

Immunofluorescence (IF) assay used to visualize the activities of pro-apoptotic proteins including BAX, caspase-3 (CASP-3) and P53 in control (cells alone), laser (cells + laser alone) at 5 J/cm^2 and Lipo@BBR (10 μg/mL) + laser groups of cells after 24 h of treatment (Fig. 5). Activity of BAX, CASP-3 and P53 proteins post-PDT in Lipo@BBR + laser group (H, I and J) have increased in comparison with control (F), laser alone (G). The non-toxic dose of Lipo@BBR (10 μg/mL) in PDT with 405 nm laser irradiation caused triggering of apoptotic cell death in A549 spheroid cells.

4. Discussion

The spheroid cell culture in comparison with monolayer mimic *in vivo* conditions due to gap junction, cellular matrix and resistance against therapy [32,33]. Using of lipid nanoparticles (LNP) is a strategy in passive and active drug delivery and cancer therapy that has been approved by the Food and Drug Administration (FDA) [34,35].

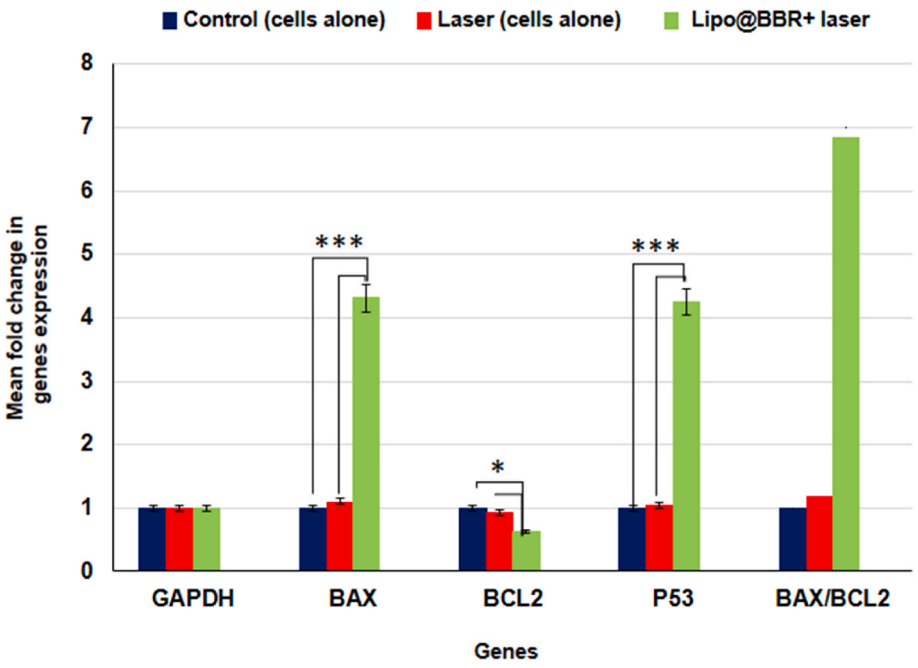

Fig. 4. The gene expression in various groups of A549 spheroid cells including control (cells alone) (blue color), laser (cells + laser) (red color) and Lipo@BBR + laser (green color) at 24 h post-PDT by RT-qPCR technique. The mRNA expression level of BAX, BCL2 and P53 in the treated group with Lipo@BBR + laser relative to the control and laser alone, are significant (*$p < 0.05$ for BCL2, ***$p < 0.01$ for BAX and P53). Moreover, BAX/BCL2 ratio as apoptosis index has been increased (6.8) in Lipo@BBR + laser group, however, BAX/BCL2 ratio fold change for control, and laser was 1 and 1.19, respectively.

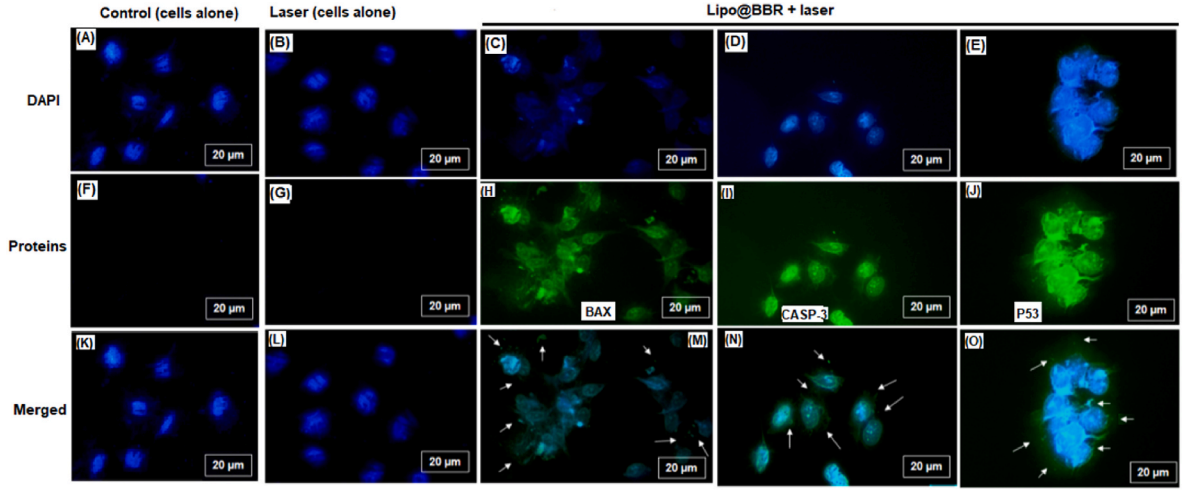

Fig. 5. BAX, CASP-3 and P53 protein activities in A549 spheroid cells for various groups such as control (cells alone) (F), laser alone (cells + laser alone) (G) and Lipo@BBR + laser, (H, I and J). DAPI stained nucleus with blue fluorescence while BAX, CASP-3 and P53 proteins stained green-FITC fluorescence and. No apoptotic proteins activities seen in control and laser alone groups (F and G). In contrast, increased activity of BAX and CASP-3 and P53 seen in Lipo@BBR (10 µg/mL) + laser (5 J/cm^2) group of cells (H, I, J) compared to control cells (F and G). (40x magnification and 20 µm scale bars).

Liposomal nanoformulations are a highly versatile and effective strategy for controlled drug delivery. By encapsulating therapeutic agents (such as drugs, proteins, or nucleic acids) in liposomes, drug release can be controlled and tailored for a specific therapeutic need [36]. BBR is a natural photosensitizer used in PDT applications, which has excellent potential to absorb light at 344–422 nm wavelength (a maximum absorption is 418 nm) which this information has been confirmed in our previous publication and others studies [19,37]. Additionally, BBR showed significant antitumor effects against breast cancer [38]. But BBR showed low water solubility and uptake by cells [39,40], hence, in this study we used liposomes as a carrier to improve permeability of BBR and its efficiency in PDT on lung cancer spheroids. Thin-film hydration was used synthesis liposomes and load BBR on liposomes. Afterward, UV–Vis spectroscopy confirmed one peak at 210 nm for lipids and three peaks for BBR at 250, 350 and 430 nm in Lipo@BBR complex. The maximum uploading of BBR in liposomes was (89 ± 2 %). Similar studies confirmed above specific peaks for lipids and BBR [41,42]. The encapsulation efficiency (%EE) of BBR in our study is close to other studies that they have reported 92.59 %, 28.7 % and 90.3 %, respectively [43-45].The surface charge of Lipo@BBR nanocomplex was negative and zeta potential was acceptable (−10.7) at pH of 6.8 (tumor pH). Hence, negative charge helps stability and affinity of nanoparticles to cells and prevent aggregation. These results have been confirmed by similar studies [44,45]. Due to electrostatic repulsion between the

liposomes (−10.7), the average size of Lipo@BBR determined by DLS was 82.7 ± 6.5 nm which is a little larger than the size determined by TEM (56.99 ± 3.74 nm) and this could be due to a little aggregation of the liposomes [44-46]. FTIR showed specific peaks for liposomes and BBR including 1250 (C–O of ester groups), 1459 (CH_2 of alkyl groups), 1736 (C═O of ester groups) and 2907 cm^{-1} (symmetric CH_2 stretching of the alkyl groups) and additionally, EDS spectra from SEM confirmed structural groups of BBR as well as lipids in Lipo@BBR complex [19,47,48].

To promote high PDT efficiency, safe dose of Lipo@BBR (10 μg/mL) and 70 mW irradiation used to apply 5 J/cm^2 in fractionated PDT. The concept behind this regime and dose rate of laser help re-oxygenation of cells and high PDT outcomes, according literature [49-51]. MTT assay showed that Lipo@BBR (contain 15 μM of BBR) does not present significant cytotoxicity in low doses (<10 μg/mL) on A549 spheroid cells but post-PDT (5 J/cm^2) viability reduced to 48.2 ± 3 %. Moreover, the spheroid volumes from 825.23 μm decreased to 413.53 μm after five sessions (5 J/cm^2 in each session) of PDT. Furthermore, compared to the control and laser groups alone, the colony formation assay demonstrated a significant reduction in cell viability in the Lipo@BBR + laser group. This indicates that A549 cells lost their capacity to proliferate and form colonies post-PDT. An *in vitro* study by Qi Hw et al. reported the IC_{50} of BBR powder on A549 cell proliferation using MTT assay was 56.15 ± 3.14 μM [52]. Similarly, Chen and colleagues noted that 40–120 μM of free BBR power caused significant anticancer activity in A549 cells by supress colony formation and protein expression of BCL-2 and BAX [53]. While Paudel et al. reported nanoformulation of BBR (berberine-loaded liquid crystalline nanoparticles (LCNs) is more effective (5 time) than free BBR. They found that BBR-LCNs formulation inhibited significant of A549 cell growth and colony formation at a dose of 2.5 and 5 μM [20]. However, to investigate the mechanism of cell death and apoptotic induced by Lipo@BBR in PDT, RT-qPCR and IF assays were performed. RT-qPCR data showed that BAX and P53 are upregulated while BCL2 expression is downregulated significantly. However, BAX/BCL2 ratio as apoptotic index in Lipo@BBR + laser groups was highest (6.8-fold increase). Several studies presented BAX/BCL2 rate as apoptotic index in cell death mechanism [54-57]. Yousefi et al. reported that over-expression of BAX, CASP3 and down-regulation of BCL2 were noted using Methylene blue (MB) in PDT on HN5 SCC cell line [58]. Other study by Devarajan and colleagues showed BBR has remarkable photosensitizing effect in PDT via apoptosis cell death and increase in BAX/BCL2 ratio [57]. Moreover, Ho et al. used BBR in PDT on SCC-4 human tongue cancer cells and their findings showed that BBR promoted apoptosis via mitochondrial damage, release cytochrome C and increasing in BAX/BCL2 ratio [59]. Additionally, IF images illustrated that BAX, CASP3-3 and P53 activities were higher in Lipo@BBR + laser group. Activation of apoptotic proteins by free form of BBR in PDT was reported by several studies. For instance, Lopes et al., showed BBR induced apoptosis and autophagy cell death in renal cell carcinoma in combination PDT. Their findings showed that BBR in PDT promoted activity of CASP3 in three different cell lines of renal cell carcinoma including ACHN, 786-O and HK-2 ,significantly [60]. Another study by Wang et al., illustrated that BBR-PDT caused to overcome of drug resistance in melanoma cancer (A375, M8, SK-Mel-19) to cisplatin via over expression of pro-apoptotic protein BAX, CASP3 and decrease in expression of anti-apoptotic protein BCL2 in melanoma cancer [61]. Furthermore, Katiyar et al., reported BBR can supress lung tumor growth *in vitro* and *in vivo* via P53 activation [62]. They tested effects of BBR on P53-positive and p53-deficient non-small cell human lung cancer cells *in vitro* and *in vivo*. Their results shown that BBR in PDT induced P53 expression in A549 cells as a common suppressor gene in cells. All these studies mentioned that free form of BBR does not show significant toxicity in low concentration (<20 μM). To overcome some of the limitations of free BBR such as water solubility and bioavailability, significant role of BBR nanoformulation in PDT has been reported in several studies. For instance, Jia et al. reported that Lipo@BBR nanoformulation improved the oral bioavailability of BBR in rat by 23.47 times in comparison with free BBR [45]. Other similar report by Comincini and co-workers illustrated that Lipo@BBR promoted PDT outcomes on glioblastoma multiforme (GBM) cancer via increase of internalization and cell death [40]. They reported BBR NPs in low concentrations did not illustrate cell death in T98G cells but in PDT caused 50 % reduction of colongenic ability of T98G cells. Nonetheless, our findings are validated by citing all of the aforementioned studies. While in comparison to monolayer cell culture, spheroid cell culture due to cell gap junction and extracellular matrix has resistance to treatment [33], using Lipo@BBR nanoformulation in fractionated PDT could be an effective strategy to overcome resistance of cancer against treatment. Some factors, including reoxygenation, degree of light penetration, PS distribution, and immunological response, may be responsible for the shrinkage and size reduction of A549 spheroid cells in fractionated PDT [7,63]. Hence, further investigation of this study could focus on hypoxia and biological markers *in vitro* and *in vivo*. Therefore, for more investigation in future, laser can be applied to machining in engineering to compare biological findings with others previous literature, moreover, laser can be applied for synthesized nanoparticles [64,65]. Additionally, the authors recommend using Lipo@BBR in PDT combined with other common treatment such as radiotherapy and immunotherapy could be a strategy to show synergistic effect on lung cancer [38]. Furthermore, since machine learning and artificial intelligence (AI) are play critical role in various fields of sciences [66,67], our findings can be evaluated and compared by machine learning and artificial intelligence (AI) for further research in cancer therapy. For this aim various algorithms such as Multi Objective Bat algorithm (MOBA), Response surface methodology (RSM) and D-optimal design approach via advanced machine learning (ML) techniques can be employed for characterization of nanoparticles such as particle size, shape, surface area [68]. Additionally, our study can also be conducted in Silico models, or computational simulation using Gleevec, Agent-Based Models and Partial Differential Equations (PDE) and the cBioportal web tool, since these tools have been used extensively in medical research to diagnose and treatment of cancer via identify biomarkers, gene expression and metabolism markers [69,70]. In Silico, or computational simulation offers a number of benefits, including tumor size prediction before and after treatment, lower costs and quicker findings than laboratory such as *in vitro*, *in vivo* tests as well as clinical [69,71]. Finally, the groups, sample selection and doses along irradiation parameters should also be extensive and optimized for future research, since this would affect the study's overall findings and conclusion [72,73].

5. Conclusion

Liposomal nanoformulation of Lipo@BBR is a strategy to overcome some limitations of BBR such as low water solubility and low uptake by cells. Furthermore, liposomal nanoformulation of BBR enhances anticancer effects of free BBR. However, BBR in low concentrations has low side effects on normal cells and liposome could be a strategy to delivery BBR to tumor cells. Our findings showed that safe dose of BBR (15 μM) on liposomes (Lipo@BBR) (10 μg/mL) can be employed in fractionated PDT in 5 sessions that the results of cell death, gene and protein expression increased significantly in comparison with control groups such in dark toxicity (cells alone without treatment) and laser group (cells alone treated by 5 J/cm^2). Lipo@BBR in fractionated PDT can improve treatment outcomes and suppress A549 spheroid cells in a few sessions of PDT. Hence, fractionated PDT promotes PDT efficiency by giving A549 spheroids an opportunity to be reoxygenated as well as more uptake of Lipo@BBR as photosensitizer during each session. Even though this study required additional experiments, such as drug release to characterize Lipo@BBR and western blotting to assess molecular response, the authors advise employing the Lipo@BBR nanocomplex in PDT fractionation, and further *in vivo* research is required to confirm the precise mechanism. Furthermore, PEGylated liposomes of Lipo@BBR

could help to target delivery of BBR to cancer cells.

CRediT authorship contribution statement

Kave Moloudi: Writing – original draft, Methodology, Formal analysis, Conceptualization. **Heidi Abrahamse:** Writing – review & editing, Supervision, Project administration, Funding acquisition. **Blassan P. George:** Writing – review & editing, Supervision, Project administration, Funding acquisition.

Funding

This work is based on the research funded by the South African Research Chairs initiative of the Department of science and technology and National Research Foundation (NRF) of South Africa (Grant No. 98337), South African Medical Research Council (Grant No. SAMRC EIP007/2021), as well as grants received from the NRF Research Development Grants for Y-Rated Researchers (Grant No: 137788), University Research Committee (URC), University of Johannesburg, and the Council for Scientific Industrial Research (CSIR) -National Laser Centre (NLC).

Declaration of competing interest

The authors declare the following financial interests/personal relationships which may be considered as potential competing interests: Authors declare that they have no known competing financial interests or personal relationships that could have appeared to influence the work reported in this paper.

Acknowledgement

The authors sincerely thank the South African Research Chairs initiative of the Department of Science and Technology and the National Research Foundation (NRF) of South Africa, the South African Medical Research Council (SAMRC), and the Laser Research Centre (LRC) of the University of Johannesburg. The research reported in this review article was supported by the South African Medical Research Council (SAMRC) through its Division of Research Capacity Development under the Research Capacity Development Initiative via funding received from the South African National Treasury. The content and findings reported/illustrated are the sole deductions, views, and responsibilities of the researchers and do not reflect the official position and sentiments of the SAMRC.

References

[1] K. Moloudi, P. Sarbadhikary, H. Abrahamse, B.P. George, Understanding the photodynamic therapy induced bystander and abscopal effects: a review, Antioxidants 12 (7) (2023) 1434.
[2] A.-G. Niculescu, A.M. Grumezescu, Photodynamic therapy—an up-to-date review, Appl. Sci. 11 (8) (2021) 3626.
[3] A. Chota, B.P. George, H. Abrahamse, Recent advances in green metallic nanoparticles for enhanced drug delivery in photodynamic therapy: a therapeutic approach, IJMS 24 (5) (2023) 4808.
[4] K. Moloudi, H. Abrahamse, B.P. George, Nanotechnology-mediated photodynamic therapy: focus on overcoming tumor hypoxia, Wiley Interdisciplinary Reviews: Nanomedicine and Nanobiotechnology 16 (1) (2024) e1937.
[5] Y. Wan, L.H. Fu, C. Li, J. Lin, P. Huang, Conquering the hypoxia limitation for photodynamic therapy, Adv. Mater. 33 (48) (2021) 2103978.
[6] Y. Sun, D. Zhao, G. Wang, Y. Wang, L. Cao, J. Sun, Q. Jiang, Z. He, Recent progress of hypoxia-modulated multifunctional nanomedicines to enhance photodynamic therapy: opportunities, challenges, and future development, Acta Pharm. Sin. B 10 (8) (2020) 1382–1396.
[7] L. Hong, J. Li, Y. Luo, T. Guo, C. Zhang, S. Ou, Y. Long, Z. Hu, Recent advances in strategies for addressing hypoxia in tumor photodynamic therapy, Biomolecules 12 (1) (2022) 81.
[8] M. Scholz, A.F. Petusseau, J.R. Gunn, M.S. Chapman, B.W. Pogue, Imaging of hypoxia, oxygen consumption and recovery in vivo during ALA-photodynamic therapy using delayed fluorescence of Protoporphyrin IX, Photodiagnosis Photodyn. Ther. 30 (2020) 101790.
[9] H. Sun, W. Yang, Y. Ong, T.M. Busch, T.C. Zhu, Fractionated photofrin-mediated photodynamic therapy significantly improves long-term survival, Cancers 15 (23) (2023) 5682.
[10] K. Khan, A.U. Khan, A. Khan, M. Khan, I. Ahmad, Fractionated illumination improves the treatment outcomes of photodynamic therapy for high grade cutaneous leishmaniasis, Photodiagnosis Photodyn. Ther. 29 (2020) 101622.
[11] L.C. van Delft, P.J. Nelemans, J.P. Kessels, H. Kreukels, M.H. Roozeboom, M.J. de Rooij, K. Mosterd, E.R. de Haas, N.W. Kelleners-Smeets, Long-term efficacy of photodynamic therapy with fractionated 5-aminolevulinic acid 20% versus conventional two-stage topical methyl aminolevulinate for superficial basal-cell carcinoma, Dermatology 238 (6) (2022) 1044–1049.
[12] A. Srivastava, A. Sinha, R. Lall, R.C. Gupta, Berberine, Nutraceuticals in Veterinary Medicine, 2019, pp. 71–81.
[13] A.F. Cicero, A. Baggioni, Berberine and its role in chronic disease, Anti-inflammatory nutraceuticals and chronic, Diseases (2016) 27–45.
[14] S. Jantová, S. Letašiová, V. Brezová, L.u. Čipák, J. Lábaj, Photochemical and phototoxic activity of berberine on murine fibroblast NIH-3T3 and Ehrlich ascites carcinoma cells, J. Photochem. Photobiol., B 85 (3) (2006) 163–176.
[15] L.O. Kostjukova, V.V. Kostjukov, The electronic states and vibronic absorption spectrum of berberine in aqueous solution, Int. J. Quant. Chem. 121 (6) (2021) e26537.
[16] I. Chauhan, V. Singh, S. Majhi, M. Verma, M. Yasir, Development and validation of UV-spectrophotometric method for berberine quantification, Journal of Applied Pharmaceutical Sciences and Research 7 (2) (2024) 28–33.
[17] P. Oliveira, T. Lopes, A.C. Tedesco, P. Rahal, M. Calmon, Effect of berberine associated with photodynamic therapy in cell lines, Photodiagnosis Photodyn. Ther. 32 (2020) 102045.
[18] C.Y. Hsu, H. Pallathadka, J. Gupta, H. Ma, H.H. Al-Shukri, A. Kareem, A. H. Zwamel, Y.F. Mustafa, Berberine and berberine nanoformulations in cancer therapy: focusing on lung cancer, Phytother Res. 38 (8) (2024) 4336–4350.
[19] K. Moloudi, H. Abrahamse, B.P. George, Co-delivery of berberine and gold nanoparticles on liposomes for photodynamic therapy against 3D lung cancer cells, Materials Advances 5 (15) (2024) 6185–6195.
[20] K.R. Paudel, M. Mehta, G.H.S. Yin, L.L. Yen, V. Malyla, V.K. Patel, J. Panneerselvam, T. Madheswaran, R. MacLoughlin, N.K. Jha, Berberine-loaded liquid crystalline nanoparticles inhibit non-small cell lung cancer proliferation and migration in vitro, Environ. Sci. Pollut. Control Ser. 29 (31) (2022) 46830–46847.
[21] C.Y. Hsu, H. Pallathadka, J. Gupta, H. Ma, H.H.K. Al-Shukri, A.K. Kareem, A. H. Zwamel, Y.F. Mustafa, Berberine and berberine nanoformulations in cancer therapy: Focusing on lung cancer, Phytother Res 38 (8) (2024 Aug) 4336–4350, https://doi.org/10.1002/ptr.8255. Epub 2024 Jul 12. PMID: 38994919.
[22] L. Sun, J. Lan, Z. Li, R. Zeng, Y. Shen, T. Zhang, Y. Ding, Transforming cancer treatment with nanotechnology: the role of berberine as a star natural compound, Int. J. Nanomed. (2024) 8621–8640.
[23] Y. Panahi, M. Farshbaf, M. Mohammadhosseini, M. Mirahadi, R. Khalilov, S. Saghfi, A. Akbarzadeh, Recent advances on liposomal nanoparticles: synthesis, characterization and biomedical applications, Artificial cells, nanomedicine, and biotechnology 45 (4) (2017) 788–799.
[24] A. Narmani, R. Jahedi, E. Bakhshian-Dehkordi, S. Ganji, M. Nemati, R. Ghahramani-Asl, K. Moloudi, S.M. Hosseini, H. Bagheri, P. Kesharwani, Biomedical applications of PLGA nanoparticles in nanomedicine: advances in drug delivery systems and cancer therapy, Expet Opin. Drug Deliv. 20 (7) (2023) 937–954.
[25] A. Chota, H. Abrahamse, B.P. George, Green synthesis and characterization of AgNPs, liposomal loaded AgNPs and ZnPcS4 photosensitizer for enhanced photodynamic therapy effects in MCF-7 breast cancer cells, Photodiagnosis Photodyn. Ther. (2024) 104252.
[26] S.G. Amin, Formulation and Evaluation of Liposomes of Fenofibrate Prepared by Thin Film Hydration Technique, Long Island University, The Brooklyn Center, 2017.
[27] H. Zhang, Thin-film hydration followed by extrusion method for liposome preparation, liposomes, Methods and Protocols (2023) 57–63. Springer.
[28] T.D. Schmittgen, K.J. Livak, Analyzing real-time PCR data by the comparative CT method, Nat. Protoc. 3 (6) (2008) 1101–1108.
[29] N.K. Balasubramainian, L. Kothandaraman, T. Sathish, J. Giri, M.I. Ammarullah, Optimization of process parameters to minimize circularity error and surface roughness in fused deposition modelling (FDM) using Taguchi method for biomedical implant fabrication, Adv. Manuf. Polym. Compos. Sci. 10 (1) (2024) 2406156.
[30] H. Nolandy, M.T.S. Utomo, B.F.T. Kiono, K.F.A. Sukra, R.T. Soewono, A. T. Rahman, M.I. Ammarullah, Gravimetric approach of fuel consumption in 30% biodiesel blends fuel: cost-effective solution of real-world fuel consumption measurement, Cogent Engineering 11 (1) (2024) 2345512.
[31] M.H. Ramlee, M.I. Ammarullah, N.S. Mohd Sukri, N.S. Faidzul Hassan, M. H. Baharuddin, M.R. Abdul Kadir, Investigation on three-dimensional printed prosthetics leg sockets coated with different reinforcement materials: analysis on mechanical strength and microstructural, Sci. Rep. 14 (1) (2024) 6842.
[32] P. Järvinen, A. Bonabi, V. Jokinen, T. Sikanen, Simultaneous culturing of cell monolayers and spheroids on a single microfluidic device for bridging the gap between 2D and 3D cell assays in drug research, Adv. Funct. Mater. 30 (19) (2020) 2000479.
[33] K. Juarez-Moreno, D. Chávez-García, G. Hirata, R. Vazquez-Duhalt, Monolayer (2D) or spheroids (3D) cell cultures for nanotoxicological studies? Comparison of cytotoxicity and cell internalization of nanoparticles, Toxicol. Vitro 85 (2022) 105461.

[34] Y. Hao, Z. Ji, H. Zhou, D. Wu, Z. Gu, D. Wang, P. Ten Dijke, Lipid-based nanoparticles as drug delivery systems for cancer immunotherapy, MedComm 4 (4) (2023) e339.
[35] M. Alavi, M. Hamidi, Passive and active targeting in cancer therapy by liposomes and lipid nanoparticles, Drug metabolism and personalized therapy 34 (1) (2019) 20180032.
[36] M. Alavi, R.S. Varma, Overview of novel strategies for the delivery of anthracyclines to cancer cells by liposomal and polymeric nanoformulations, Int. J. Biol. Macromol. 164 (2020) 2197–2203.
[37] F. Carriero, Photodynamic Therapy Using the Natural Photosensitizer Berberine (BBR) and its Derivatives NAX Induces Apoptosis in Human Astrocytoma-Established Cells, 2023.
[38] Q. Zhao, Y. Jiang, S. Xiang, P.J. Kaboli, J. Shen, Y. Zhao, X. Wu, F. Du, M. Li, C. H. Cho, Engineered TCR-T cell immunotherapy in anticancer precision medicine: pros and cons, Front. Immunol. 12 (2021) 658753.
[39] W. Xiong, W. Sang, K.G. Linghu, Z.F. Zhong, W.S. Cheang, J. Li, Y.J. Hu, H. Yu, Y. T. Wang, Dual-functional Brij-S20-modified nanocrystal formulation enhances the intestinal transport and oral bioavailability of berberine, Int. J. Nanomed. (2018) 3781–3793.
[40] S. Comincini, F. Manai, M. Sorrenti, S. Perteghella, C. D'Amato, D. Miele, L. Catenacci, M.C. Bonferoni, Development of Berberine-loaded nanoparticles for astrocytoma cells administration and photodynamic therapy stimulation, Pharmaceutics 15 (4) (2023) 1078.
[41] T.T. Duong, T.T.H. Yen, L.T. Nguyen, T.-D. Nguyen, H.T. Pham, A. Raal, J. Heinämäki, Berberine-loaded liposomes for oral delivery: preparation, physicochemical characterization and in-vivo evaluation in an endogenous hyperlipidemic animal model, Int. J. Pharm. 616 (2022) 121525.
[42] I.E. Allijn, B.M. Czarny, X. Wang, S.Y. Chong, M. Weiler, A.E. Da Silva, J. M. Metselaar, C.S.P. Lam, G. Pastorin, D.P. De Kleijn, Liposome encapsulated berberine treatment attenuates cardiac dysfunction after myocardial infarction, J. Contr. Release 247 (2017) 127–133.
[43] J. Wu, C. Qi, H. Wang, Q. Wang, J. Sun, J. Dong, G. Yu, Z. Gao, B. Zhang, G. Tian, Curcumin and berberine co-loaded liposomes for anti-hepatocellular carcinoma therapy by blocking the cross-talk between hepatic stellate cells and tumor cells, Front. Pharmacol. 13 (2022) 961788.
[44] A. Calvo, E. Moreno, E. Larrea, C. Sanmartín, J.M. Irache, S. Espuelas, Berberine-loaded liposomes for the treatment of Leishmania infantum-infected BALB/c mice, Pharmaceutics 12 (9) (2020) 858.
[45] J. Jia, K. Zhang, X. Zhou, J. Ma, X. Liu, A. Xiang, F. Ge, Berberine-loaded solid proliposomes prepared using solution enhanced dispersion by supercritical CO2: sustained release and bioavailability enhancement, J. Drug Deliv. Sci. Technol. 51 (2019) 356–363.
[46] B. Roy, P. Guha, R. Bhattarai, P. Nahak, G. Karmakar, P. Chettri, A.K. Panda, Influence of lipid composition, pH, and temperature on physicochemical properties of liposomes with curcumin as model drug, J. Oleo Sci. 65 (5) (2016) 399–411.
[47] F.A. Younis, S.R. Saleh, S.S.A. El-Rahman, A.-S.A. Newairy, M.A. El-Demellawy, D. A. Ghareeb, Preparation, physicochemical characterization, and bioactivity evaluation of berberine-entrapped albumin nanoparticles, Sci. Rep. 12 (1) (2022) 17431.
[48] A. Musa, A.H. Elmaidomy, A.M. Sayed, S.I. Alzarea, M.M. Al-Sanea, E.M. Mostafa, O.M. Hendawy, M.A. Abdelgawad, K.A. Youssif, H. Refaat, Cytotoxic potential, metabolic profiling, and liposomes of Coscinoderma sp. crude extract supported by in silico analysis, Int. J. Nanomed. (2021) 3861–3874.
[49] T.M. Busch, S.M. Hahn, S.M. Evans, C.J. Koch, Depletion of tumor oxygenation during photodynamic therapy: detection by the hypoxia marker EF3 [2-(2-nitroimidazol-1 [H]-yl)-N-(3, 3, 3-trifluoropropyl) acetamide], Cancer Res. 60 (10) (2000) 2636–2642.
[50] L.G. Kuliková, Different Effects of Single and Fractionated Light Delivery Regimes in Photodynamic Therapy with Hypericin on HT-29 Cells in Vitro,.
[51] M. Arun, D. Barik, S.S. Chandran, N. Govil, P. Sharma, T.Y. Khan, R.U. Baig, B. J. Bora, B.J. Medhi, R. Kumar, Twisted helical Tape's impact on heat transfer and friction in zinc oxide (ZnO) nanofluids for solar water heaters: biomedical insight, Case Stud. Therm. Eng. 56 (2024) 104204.
[52] H.-w. Qi, L.-y. Xin, X. Xu, X.-x. Ji, L.-h. Fan, Epithelial-to-mesenchymal transition markers to predict response of Berberine in suppressing lung cancer invasion and metastasis, J. Transl. Med. 12 (2014) 1–10.
[53] Q.-q. Chen, J.-m. Shi, Z. Ding, Q. Xia, T.-s. Zheng, Y.-b. Ren, M. Li, L.-h. Fan, Berberine induces apoptosis in non-small-cell lung cancer cells by upregulating miR-19a targeting tissue factor, Cancer Manag. Res. (2019) 9005–9015.
[54] C. Li, X. Wu, R. Sun, P. Zhao, F. Liu, C. Zhang, Croton tiglium extract induces apoptosis via Bax/Bcl-2 pathways in human lung cancer A549 cells, Asian Pac. J. Cancer Prev. APJCP: Asian Pac. J. Cancer Prev. APJCP 17 (11) (2016) 4893.
[55] S. Samarghandian, M. Azimi-Nezhad, T. Farkhondeh, Thymoquinone-induced antitumor and apoptosis in human lung adenocarcinoma cells, J. Cell. Physiol. 234 (7) (2019) 10421–10431.
[56] K. Moloudi, A. Neshasteriz, A. Hosseini, N. Eyvazzadeh, M. Shomali, S. Eynali, E. Mirzaei, A. Azarnezhad, Synergistic effects of arsenic trioxide and radiation: triggering the intrinsic pathway of apoptosis, Iran. Biomed. J. 21 (5) (2017) 330.
[57] N. Devarajan, S. Jayaraman, J. Mahendra, P. Venkatratnam, P. Rajagopal, H. Palaniappan, S.K. Ganesan, Berberine—a potent chemosensitizer and chemoprotector to conventional cancer therapies, Phytother Res. 35 (6) (2021) 3059–3077.
[58] M. Yousefi, M. Koopaie, R. Karimi, F.M. Kermani, S. Kolahdooz, A. Shamshiri, Effect of photodynamic therapy on expression of HRAS, NRAS and caspase 3 genes at mRNA levels, apoptosis of head and neck squamous cell carcinoma cell line, Photodiagnosis Photodyn. Ther. 33 (2021) 102142.
[59] Y.-T. Ho, C.-C. Lu, J.-S. Yang, J.-H. Chiang, T.-C. Li, S.-W. Ip, T.-C. Hsia, C.-L. Liao, J.-G. Lin, W.G. Wood, Berberine induced apoptosis via promoting the expression of caspase-8,-9 and-3, apoptosis-inducing factor and endonuclease G in SCC-4 human tongue squamous carcinoma cancer cells, Anticancer Res. 29 (10) (2009) 4063–4070.
[60] T.Z. Lopes, F.R. de Moraes, A.C. Tedesco, R.K. Arni, P. Rahal, M.F. Calmon, Berberine associated photodynamic therapy promotes autophagy and apoptosis via ROS generation in renal carcinoma cells, Biomed. Pharmacother. 123 (2020) 109794.
[61] X. Wang, Q. Gong, C. Song, J. Fang, Y. Yang, X. Liang, X. Huang, J. Liu, Berberine-photodynamic therapy sensitizes melanoma cells to cisplatin-induced apoptosis through ROS-mediated P38 MAPK pathways, Toxicol. Appl. Pharmacol. 418 (2021) 115484.
[62] S.K. Katiyar, S.M. Meeran, N. Katiyar, S. Akhtar, p53 cooperates berberine-induced growth inhibition and apoptosis of non-small cell human lung cancer cells in vitro and tumor xenograft growth in vivo, Molecular Carcinogenesis: published in cooperation with the University of Texas MD, Anderson Cancer Center 48 (1) (2009) 24–37.
[63] L. Larue, B. Myrzakhmetov, A. Ben-Mihoub, A. Moussaron, N. Thomas, P. Arnoux, F. Baros, R. Vanderesse, S. Acherar, C. Frochot, Fighting hypoxia to improve PDT, Pharmaceuticals 12 (4) (2019) 163.
[64] M.I. Ammarullah, R. Hartono, T. Supriyono, G. Santoso, S. Sugiharto, M. S. Permana, Polycrystalline diamond as a potential material for the hard-on-hard bearing of total hip prosthesis: von Mises stress analysis, Biomedicines 11 (3) (2023) 951.
[65] M. Farooq, S. Anwar, H. Bhatti, M. Kumar, M. Ali, M. Ammarullah, Electric discharge machining of Ti6Al4V ELI in biomedical industry: parametric analysis of surface functionalization and tribological characterization, Materials 16 (2023) 4458.
[66] P. Rao, S. Dhoria, S. Patro, R. Gopidesi, M. Alkahtani, S. Islam, M. Vijaya, J. Jayanthi, M. Khan, A. Razak, Artificial intelligence based modelling and hybrid optimization of linseed oil biodiesel with graphene nanoparticles to stringent biomedical safety and environmental standards, Case Stud. Therm. Eng. 51 (2023) 103554, 2023.
[67] M.R. Karim, S.M. Ashiquzzaman Nipu, M.S. Hossain Shawon, R. Kumar, S. Salman, A. Verma, E.-S.M. Sherif, S. Islam, M.I. Ammarullah, Machinability investigation of natural fibers reinforced polymer matrix composite under drilling: leveraging machine learning in bioengineering applications, AIP Adv. 14 (4) (2024).
[68] P.M. Rao, S.H. Dhoria, S.G.K. Patro, R.K. Gopidesi, M.Q. Alkahtani, S. Islam, M. Vijaya, J.L. Jayanthi, M.A. Khan, A. Razak, Artificial intelligence based modelling and hybrid optimization of linseed oil biodiesel with graphene nanoparticles to stringent biomedical safety and environmental standards, Case Stud. Therm. Eng. 51 (2023) 103554.
[69] H. Kunhabdulla, R. Manas, A.K. Shettihalli, C.R.M. Reddy, M.S. Mustak, R. Jetti, R. Abdulla, D.R. Sirigiri, D. Ramdan, M.I. Ammarullah, Identifying biomarkers and therapeutic targets by multiomic analysis for HNSCC: precision medicine and healthcare management, ACS Omega 9 (11) (2024) 12602–12610.
[70] L.B. Edelman, J.A. Eddy, N.D. Price, Wiley Interdiscip. Rev. Syst. Biol. Med. 2 (4) (2010) 438–459. In silico models of cancer.
[71] M.I. Ammarullah, G. Santoso, S. Sugiharto, T. Supriyono, D.B. Wibowo, O. Kurdi, M. Tauviqirrahman, J. Jamari, Minimizing risk of failure from ceramic-on-ceramic total hip prosthesis by selecting ceramic materials based on tresca stress, Sustainability 14 (20) (2022) 13413.
[72] M.I. Maula, M.I. Ammarullah, H.N. Fadhila, I.Y. Afif, H. Hardian, J. Jamari, T. I. Winarni, Comfort evaluation and physiological effects/autonomic nervous system response of inflatable deep pressure vest in reducing anxiety, Heliyon 10 (16) (2024) e36065.
[73] G. Kaur, J. Kaur, A. Sharma, A. Jain, R. Kumar, M. Alsubih, S. Islam, M. I. Ammarullah, Techno-economic investigation and empowering rural resilience through bioengineering: a case study on self-sustainable village energy models, Int. J. Low Carbon Technol. 19 (2024) 1275–1287.